Simulation of the Effect of the Main Wing on the Tail Differential Pressure Force of an Aircraft Based on the Spalart-Allmaras Model

Jialuo Hong[1*]

[1] School of Physical Science and Technology, Nanjing Normal University, Nanjing, 210000, China
*07210227@nnu.edu.cn

Abstract. To investigate the characteristics of the differential pressure force on the tailplane which is in the trailing edge of the main wing. In this paper, Ansys Fluent software is used to simulate the characteristics of the differential pressure force on the tailplane when aircraft with different tail heights are performing 15° elevation manoeuvres. In this paper, the main wing of the aircraft adopts the NACA2412 airfoil and is simulated using the Spalart-Allmaras model. The results show that the obstruction effect of the main wing on the airflow, as well as the vortex at the rear end of the main wing can greatly affect the pressure distribution on the tail surface. In particular, the flow field near the wake cannot reach a steady state but fluctuates within a certain range, and the position of the wake has a strong relationship with the mean value of the fluctuation and the intensity of the fluctuation. In addition, the lift applied to the tail in the wake varies significantly, and the lift applied to the tail is larger when it is at the lower boundary of the main wing wake and in the middle of the wake. This study fills the gap of research in the related field and provides help for the aerodynamic shape design of small aircraft.

Keywords: Ansys Fluent, main wing, tail, Spalart-Allmaras, vortex shedding.

1 Introduction

Small aircraft have a wide range of applications in a number of fields, including recreational flights, flight training, agricultural operations, aerial surveying and remote sensing, and emergency medical services, etc. Their characteristics include overall lightness, ease of operation, lower cost, and more flexible use. With the iterative upgrading of small aircraft in terms of aeronautical materials, avionics systems and power systems, their performance and range of applications have been enhanced to a greater extent, and they occupy an important position in the current general-purpose market.

From the point of view of the overall aerodynamic layout design of an aircraft, the design of the tail and the wing are interrelated, and both of them jointly determine the aerodynamic balance and stability, manoeuvrability, aerodynamic efficiency,

Y. Yue (ed.), *Proceedings of the 2024 International Conference on Mechanics, Electronics Engineering and Automation (ICMEEA 2024)*, Advances in Engineering Research 240,
https://doi.org/10.2991/978-94-6463-518-8_3

aerodynamic layout, structure and weight distribution of the aircraft, etc., and the above factors are particularly important for the safety of the aircraft in flight. In the study of aerodynamic characteristics of aircraft, the mainstream research method is numerical method. Numerical methods simulate the aerodynamic response of an aircraft by predicting and analysing complex flows, which can reduce the need for experiments in wind tunnels, improve design efficiency, reduce costs, and enhance the safety and reliability of aircraft design.

There are many articles on the interaction of the main wing tail. Pan and Cheng [1] investigated the aerodynamic interference and aeroelastic properties of the main wing on the tail in a transonic flow field by using a windward unstructured Euler solver based on the Roe approximation of the Riemann solver. It was found that the wing can slow down the airflow approaching the tail and increase the tremor boundary of the tail, while the downwash flow generated by the wing may increase the effective angle of attack of the tail. Sensburg et al. [2] found that the tremor is entirely caused by aerodynamic disturbances through theoretical and experimental validation based on a variable geometry aircraft model. Tuncer et al. [3] used a regional Navier- Stokes solver to compute the unsteady flow field and discretise the computational domain by overlapping uniform grids to investigate the unsteady aerodynamic effects of a flapping/static aerodynamic combination (i.e., main and tail) in low subsonic flow. Majeed [4] predicted the flow characteristics between two sets of wings, the main wing and the tail, using a low-order surface element method. Robert et al. [5] applied the theory to a practical case and investigated the transient effect of the main wing wake on the horizontal tail lift. Hoang et al. [6] explored the effect of the downwash flow of an aircraft's main wing on the pressure differential force characteristics of a horizontal tail, and found that the downwash flow of the main wing produces an additional lift on the tail, and as the angle of attack of the main wing increases, the strength of the wingtip vortices and the downwash angle also increase. Mckenn et al. [7] used particle image velocimetry and found that the impact of a directional vortex with a downstream aerodynamic surface leads to non-stationary loading and affects the change in the lift-to-drag ratio. Qiu Ju and Sun Qin [8] discussed two methods for calculating aerodynamic loads: the dual lattice method (DLM) and computational fluid dynamics (CFD), and found that the aerodynamic loads of a horizontal tail are not only related to its shape and elastic deformation under external loads, but also determine the structural distribution, structural strength, and stiffness design. Jun-Duo Zhang et al [9] used an adaptive mesh-based large vortex simulation (LES) method and found that the vortex generated by the horizontal tail is the weakest and dissipates the fastest, while the flap vortex is the strongest and is able to induce the wingtip vortex to merge with it. The above literature highlights the important influence of the main wing on the aerodynamic characteristics of the tail, especially in the study of flutter analysis and non-constant loading, where the interaction between the main wing and the tail cannot be ignored. The traditional studies focus on the wingtip vortices in terms of aerodynamic disturbances, and lack of studies on the effect of tail height and vortex shedding behind the main wing on the flow field. In this paper, the wing layout with different tail heights is modelled, and the flow field during each

vortex shedding cycle is simulated and visualised, which in turn leads to the causes of pressure fluctuations on the tail surface.

In this paper, a flow field simulation based on the Spalart-Allmaras model is carried out in Ansys Fluent to investigate the effect of the main wing on the differential pressure force characteristics of the tailplane at 15° elevation angle. Firstly, in this paper, the wing is first modeled to explore the mesh division around the wing, then give the control equations and the fixed solution conditions used in the simulation, extract the pressure distribution on the surface of the tail after calculation, and then get the mean value of the pressure fluctuation and the intensity of the fluctuation, and finally analyse the effect of the manoeuvre with 15° elevation angle on the lift applied to the tail at different tail positions. In this paper, the mode of vortex shedding from the main wing and the way it affects the pressure on the tail surface are analysed by means of flow field visualisation, and then the causes of the pressure distribution on the tail surface are analysed, which can help the aerodynamic shape design of small aircraft and reduce the potential risk of the aircraft when manoeuvring at small elevation angles.

2 Model Simulation

2.1 Wing Model

The main wing is selected from the NACA2412 wing type which is widely used in small aircraft, with a chord length of 1 m. The wing model and coordinates are shown in Fig. 1.

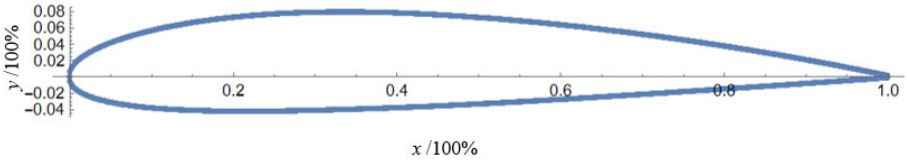

Fig. 1. Wing model (Photo/Picture credit : Original)

The tail is set up as a rectangle with a length of 0.5 m and a height of 0.02 m. Its spacing from the main wing is 1.5 m. In this paper, six scenarios with vertical distances of 0 m, 0.2 m, 0.4 m, 0.6 m, 0.8 m, and 1.0 m is discussed.

2.2 Meshing

The above wing data points are imported into ICEM CFD to establish the wing model. The flow field is divided into two pieces, the maximum size of the external mesh is 0.1m, the maximum size of the internal mesh is 0.01m, and 10 layers of encrypted mesh are set on the surface of the wing, with the mesh height of 0.001 m.

The overall mesh division is shown in Fig. 2, and the encryption of the mesh of the main wing and the tail is shown in Fig. 3.

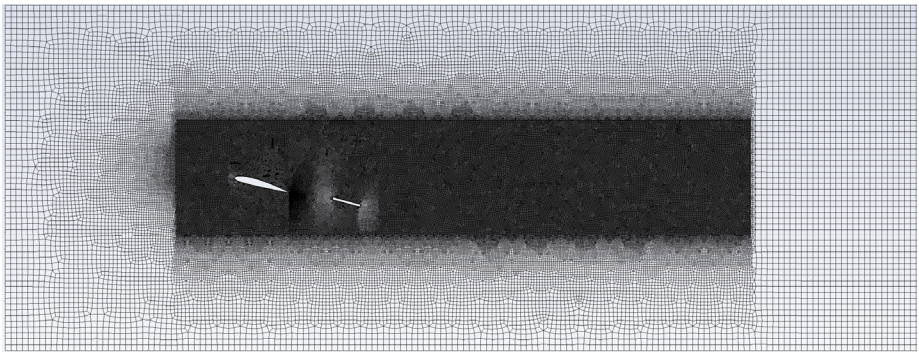

Fig. 2. Overall meshing (Photo/Picture credit : Original)

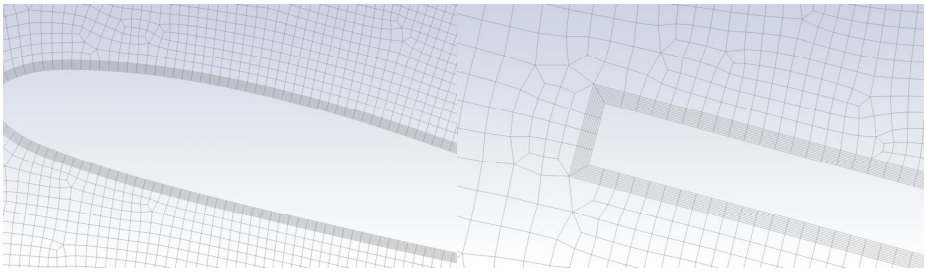

(a) (b)

Fig. 3. Mesh division of the main wing and the tail. (a) Main wing; (b) Tail (Photo/Picture credit : Original)

2.3 Governing Equation

The Spalart-Allmaras model is based on the linear viscous vortex assumption and uses the following equation to calculate the turbulent viscosity.

$$\nu_t = \tilde{\nu} f_{v1} \tag{1}$$

Where $\tilde{\nu}$ is the quantity to be solved by the transport equation. The viscous damping function f_{v1} is related to the turbulent viscosity ratio χ and is defined as

$$f_{v1} = \frac{\chi^3}{\chi^3 + C_{v1}^3} \tag{2}$$

The turbulent viscosity ratio is defined as

$$\chi = \frac{\tilde{\nu}}{\nu} \tag{3}$$

The transport equation for $\tilde{\nu}$ can be expressed in the following form

$$\frac{\partial \tilde{v}}{\partial t} = M(\tilde{v}) + P(\tilde{v}) + D(\tilde{v}) + T \tag{4}$$

where $M(\tilde{v})$ denotes diffusion and convection

$$M(\tilde{v}) = -\nabla \cdot (\tilde{v}u) + \frac{1}{\sigma}\left\{\nabla\cdot\left[(v+\tilde{v})\nabla\tilde{v}\right]+C_{b2}\left(\nabla\tilde{v}\right)^2\right\} \tag{5}$$

$P(\tilde{v})$ denotes production.

$$P(\tilde{v}) = C_{b1}(1-f_{t2})\tilde{S}\tilde{v} \tag{6}$$

$D(\tilde{v})$ denotes wall destruction.

$$D(\tilde{v}) = \left(C_{w1}f_w - \frac{C_{b1}}{\kappa^2}f_{t2}\right)\left(\frac{\tilde{v}}{d}\right)^2 \tag{7}$$

T is for trip function

$$T = f_{t1}\Delta u^2 \tag{8}$$

$\tilde{S}$ is defined as follows

$$\tilde{S} = S + \frac{\tilde{v}}{\kappa^2 d^2}f_{v2} \tag{9}$$

where S is the scalar measure of the deformation tensor, d is the distance to the wall, and f_{v2} is defined as

$$f_{v2} = 1 - \frac{\chi}{1+\chi f_{v1}} \tag{10}$$

The f_w in the Wall destruction term is defined as

$$f_w = g\left(\frac{1+C_{w3}^6}{g^6+C_{w3}^6}\right)^{\frac{1}{6}} \tag{11}$$

$$g = 9.8r + C_{w2}(r^6 - r) \tag{12}$$

$$r = \min\left(\frac{\tilde{v}}{\tilde{S}\kappa^2 d^2}, 10\right) \tag{13}$$

where σ , κ , C_{b1} , C_{b2} , C_{w1} , C_{w2} , C_{w3} , C_{v1} and C_s , are constant coefficients [10], and their default values are shown in Table 1.

Table 1. Spalart-Allmaras model constants

σ	κ	C_{b1}	C_{b2}	C_{w1}	C_{w2}	C_{w3}	C_{v1}	C_s
0.6666	0.41	0.1355	0.622	$\frac{C_{b1}}{\kappa^2}+\frac{1+C_{b2}}{\sigma}$	0.3	2.0	7.1	0.3

2.4 Solution Conditions

The inlet velocity is set to 50m/s and no-slip boundary conditions are used for the wall as well as the wing surface. In the initial state, the air velocity is 0 and the air pressure is 10^5Pa.

3 Results and Discussion

The simulation found that the flow field around the wing cannot reach a steady state but fluctuates within a certain range at 15° elevation angle and 50m/s flight speed. Taking the flow field case with a tail height of 0.2m and a simulation time of 2.90s to 3.04s as an example, the vortex changes in the main wing wake are shown in Fig. 4, with the colours representing the magnitude of the pressure and the arrows representing the direction of the velocity. From Fig. 4, it can be found that the vortex in the trailing edge of the main wing develops from the inverse pressure gradient at the upper end of the main wing. The vortex moves backward with time and gradually forms a double vortex structure, and the vortex at the rear end breaks up after leaving the main wing trailing edge for some time, forming an airflow disturbance between the main wing and the trailing edge. Then, the front end of the tail is affected by the airflow disturbance and forms a small vortex on the tail, which continues to move backwards until it breaks up and disappears. At the same time, the inverse pressure gradient on the main wing began to form, and the flow field appeared to oscillate periodically.

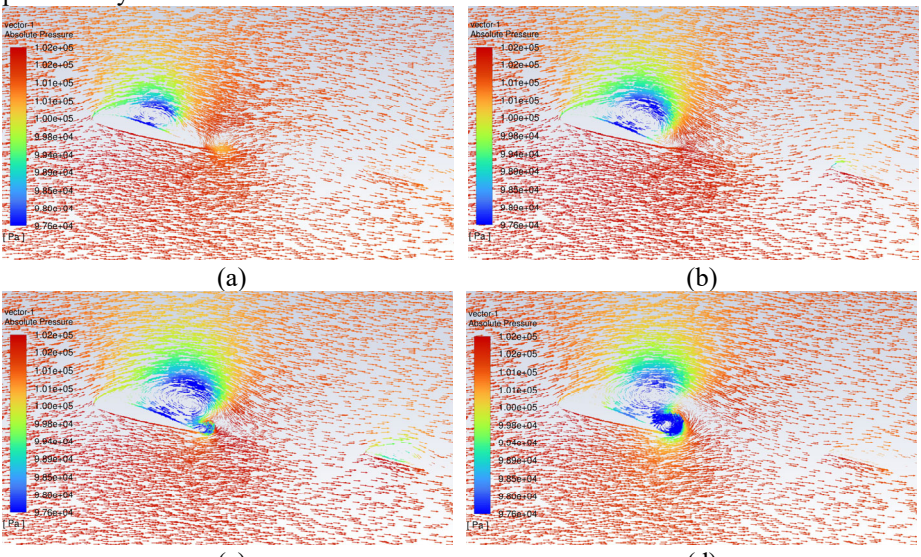

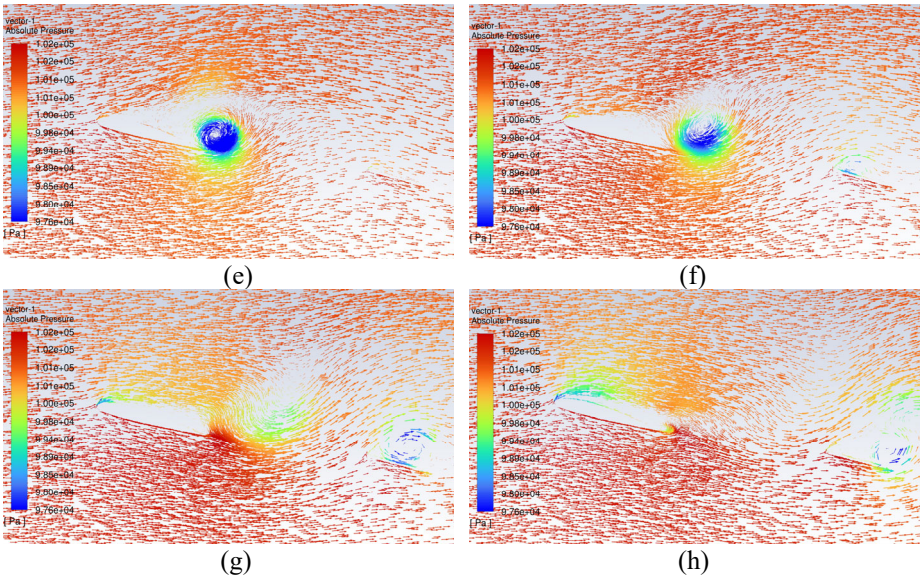

Fig. 4. Flow field simulation results. (a) Time = 2.90s; (b) Time = 2.92s; (c) Time = 2.94s; (d) Time = 2.96s; (e) Time = 2.98s; (f) Time = 3.00s; (g) Time = 3.02s; (h) Time = 3.04s; (Photo/Picture credit: Original)

After a period of unsteady fluctuation, the flow field enters a steady fluctuation state, and the pressure at the rear end of the wake varies with time as shown in Fig. 5.

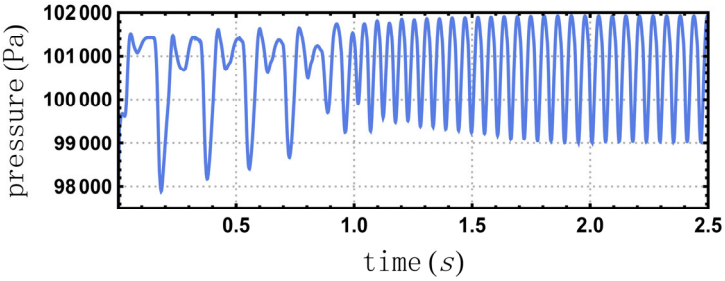

Fig. 5. Variation of pressure at the trailing edge of the tail fin with time. (Photo/Picture credit : Original)

In this study, the data of steady fluctuation state of the flow field are selected for analysis to obtain the distribution of the mean value of the pressure and the distribution of the fluctuation intensity under different tail heights. As shown in Figs. 6-11.

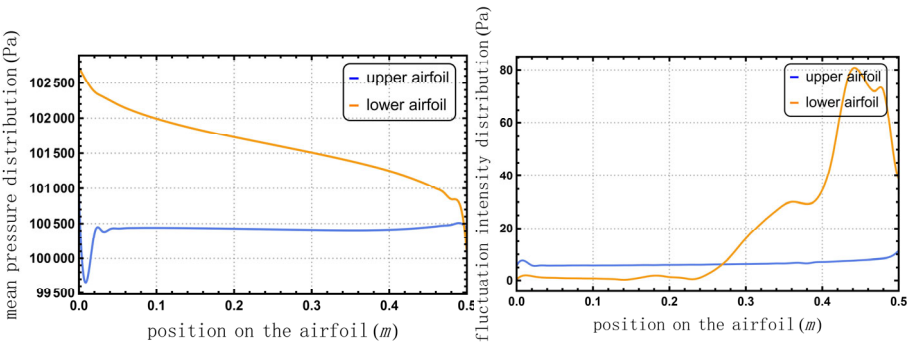

(a) (b)

Fig. 6. Mean pressure distribution and pressure fluctuation intensity on the tail fin (h=0.0m). (a) Mean pressure distribution; (b) Pressure fluctuation intensity (Photo/Picture credit : Original)

As shown in Fig. 6, when the height of the tail is 0 m, the pressure difference is large at the front end of the tail and small at the rear end. The sudden change in pressure on the upper surface of the leading end of the tail is due to the early separation of the boundary layer caused by the rectangular shape of the tail. The tail does not enter the wake area of the main wing, so the pressure fluctuation of the airfoil surface is small, and the pressure fluctuation of the lower surface of the rear end of the tail increases due to the high-speed airflow impacting on the lower surface of the front end of the tail, forming a high-pressure area, and the airflow is accelerated by the tail obstruction, forming a low-pressure area at the rear of the tail, and the pressure gradient leads to the pressure fluctuation of the lower surface of the rear end of the tail becomes larger.

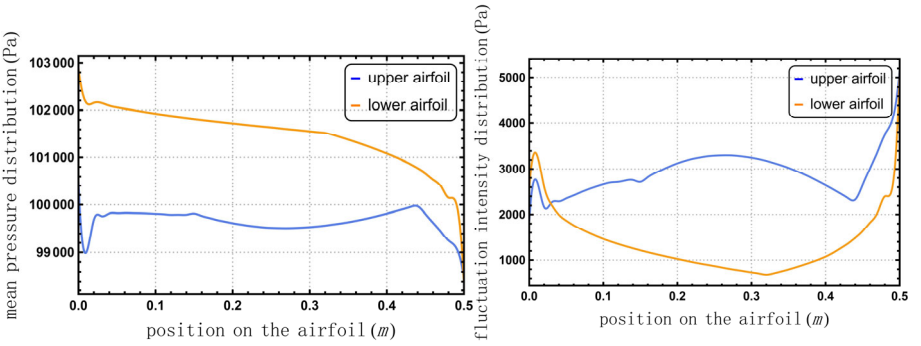

(a) (b)

Fig. 7. Mean pressure distribution and pressure fluctuation intensity on the tail fin (h=0.2m). (a) Mean pressure distribution; (b) Pressure fluctuation intensity (Photo/Picture credit : Original)

As shown in Fig. 7, when the height of the tail is 0.2m, the tail is at the lower boundary of the main wing wake, and the lower surface of the tail is still less affected by the main wing wake, while the upper surface is affected by the periodic shedding

of the main wing vortex, which forms the unevenly distributed mean and fluctuating pressure. After the main wing vortex shedding, the airflow disturbance is formed, and the disturbance is transmitted backward, resulting in the vortex on the upper surface of the tail, and the vortex moves backward until it touches the trailing edge of the tail, and the breakup of the vortex leads to the formation of an unstable low-pressure region on the upper surface of the trailing end of the tail, so the average pressure at the trailing end of the tail decreases suddenly, and at the same time, the intensity of the fluctuation increases suddenly.

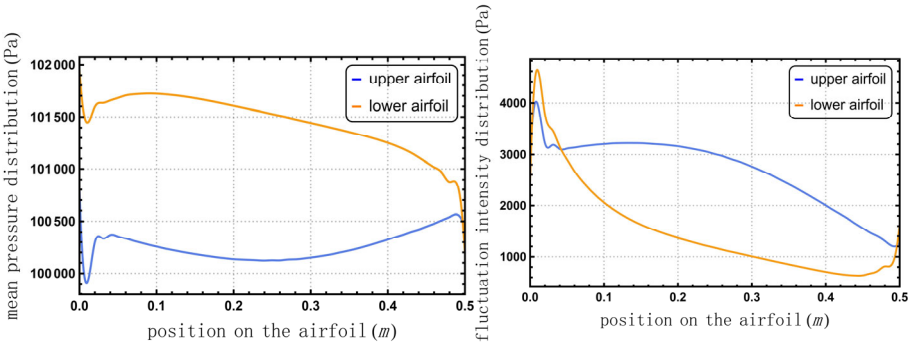

(a) (b)

Fig. 8. Mean pressure distribution and pressure fluctuation intensity on the tail fin (h=0.4m). (a) Mean pressure distribution; (b) Pressure fluctuation intensity (Photo/Picture credit : Original)

As shown in Fig. 8, when the tail height is 0.4m, the tail is at the lower end of the main wing trailing edge, and the tail height becomes higher so that the tail blocks more airflow from the main wing. Due to the blocking of the airflow at its front end, it causes the vortex on the tail to start from the front end and move smoothly to the rear end until it disappears. As a result, the intensity of fluctuations in the pressure on the tailplane does not change abruptly, but follows the pattern that the upper airfoil is more affected by the airflow and has a higher intensity of fluctuations. Unlike the case where the height of the tail is 0.2 m, there is no sudden change in the mean pressure distribution on the tail because there is no unstable low-pressure region.

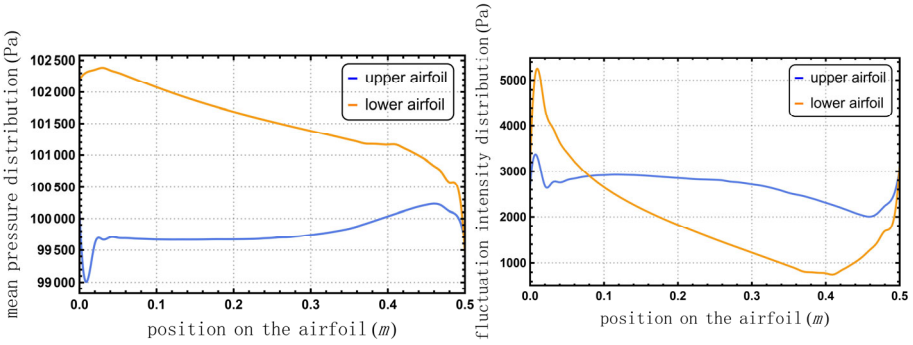

(a) (b)

Fig. 9. Mean pressure distribution and pressure fluctuation intensity on the tail fin (h=0.6m). (a) Mean pressure distribution; (b) Pressure fluctuation intensity (Photo/Picture credit : Original)

As shown in Fig. 9, when the tail height is 0.6m, the tail is in the middle of the main wing trajectory, and the lower surface of the tail is affected by the vortex of the main wing, and the magnitude of the pressure fluctuation at the front end increases, while the pressure fluctuation at the rear end does not change significantly because the vortex cannot be formed at the lower end of the tail. For the upper surface, the vortex still moves smoothly to the aft end until it disappears, so the fluctuation intensity distribution is similar to that of the case with a tail height of 0.6m. Since there is no sudden change of vortex, the pressure distribution of the tail has only small fluctuations, and its upper and lower surfaces are still characterised by a large pressure difference at the front end and a small pressure difference at the rear end.

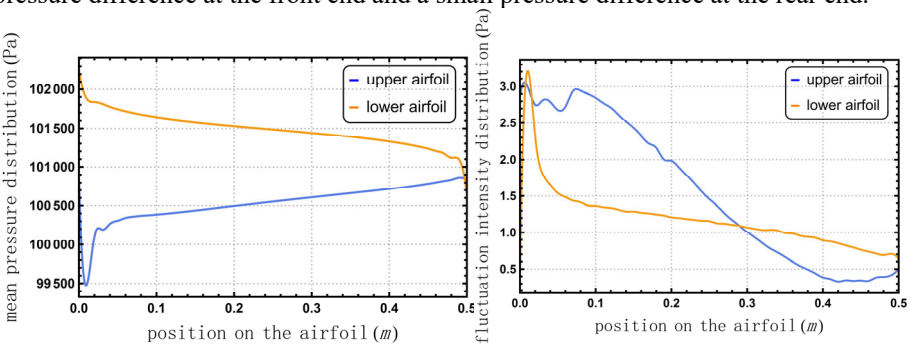

(a) (b)

Fig. 10. Mean pressure distribution and pressure fluctuation intensity on the tail fin (h=0.8 m). (a) Mean pressure distribution; (b) Pressure fluctuation intensity (Photo/Picture credit : Original)

As shown in Fig. 10, when the tail height is 0.8 m, the tail is at the upper end of the main wing trailing edge. Since the high-pressure area formed by the tail's blockage of the airflow is located directly behind the main wing, which hinders the shedding of the vortex, the tail is not affected by the periodic airflow disturbance, and the fluctuation of the pressure is extremely small. There was also no piece of low-pressure area formed at the front end of the lower wing of the tail, and its average pressure distribution was relatively uniform. In addition, the average pressure on the upper airfoil of the tail is higher than in other cases due to the absence of vortex-induced airflow disturbances.

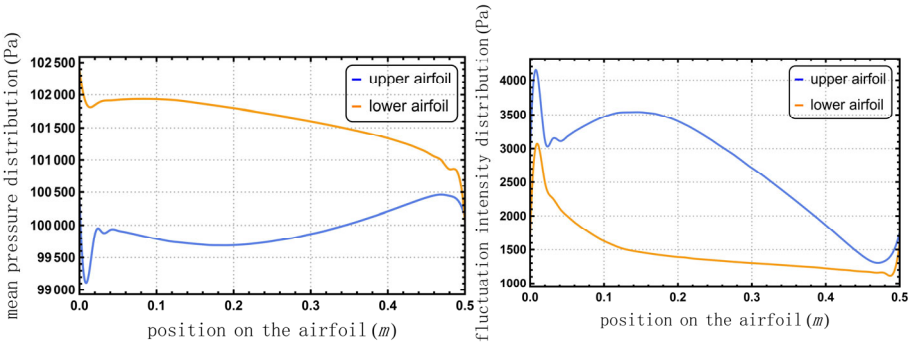

(a) (b)

Fig. 11. Mean pressure distribution and pressure fluctuation intensity on the tail fin (h=1.0m). (a) Mean pressure distribution; (b) Pressure fluctuation intensity (Photo/Picture credit : Original)

As shown in Fig. 11, when the tail height is 1.0 m, the tail is at the upper boundary of the main wing trailing edge. The position of the high-pressure area at the front of the tail is higher than the height of the vortex with the back of the main wing, so the vortex still undergoes periodic shedding, forming periodic pressure fluctuations on the surface of the tail. However, because of the higher position of the tailplane, the lower airfoil surface becomes less disturbed by the airflow, so the intensity of the pressure fluctuation becomes smaller. The upper airfoil surface is affected by the vortex and still shows the characteristics of strong fluctuation in the middle and weak fluctuation at both ends. Due to the appearance of the vortex, the average pressure of the upper airfoil decreases again, showing the characteristics of high at both ends and low in the middle.

The aircraft tail is subjected to different lift forces in the main wing wake, and the relationship between the lift forces and the tail height is shown in Fig. 12.

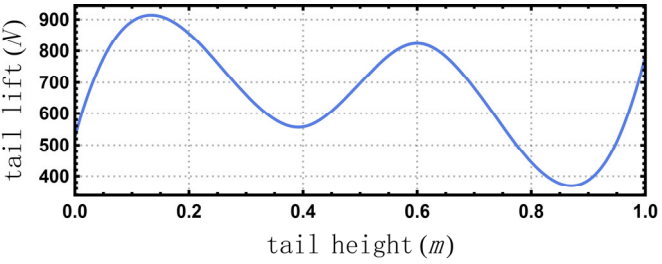

Fig. 12. Tail fin height vs. lift. (Photo/Picture credit: Original)

Entering the trailing zone of the main wing does not simply result in a decrease in the lift applied to the tail, but causes the relationship between tail height and lift to be characterised by multiple peaks. The first peak of lift occurs at 0.3m of the tail height, which is due to the tail encountering the high-speed airflow at the lower end of the main wing, and the direct impact of the high-speed airflow leads to the high pressure of the tail's lower airfoil surface, thus generating high lift. The second peak occurs at the tail height of 0.6m, this is due to the high pressure area at the front of the tail is at

the same height with the vortex on the main wing, the high pressure area hinders the vortex shedding, thus avoiding the pressure fluctuation on the tail surface and improving the lift applied to the tail. The increase in lift at the tail height of 1.0m is due to the fact that the tail is gradually detached from the trailing edge area of the main wing and is less affected by the vortex. In addition, the cyclic variation of vortices on the tail due to vortex shedding from the main wing resulted in lift valleys at tail heights of 0.4m and 0.85m.

According to the above study, the inverse pressure gradient on the upper part of the main wing develops into a vortex in a wind speed of 50m/s and an aircraft performing a manoeuvre with a 15° elevation angle. Only when the tail is at the top of the main wing trailing edge, the vortex cannot be shed due to the obstruction of the high-pressure area at the front of the tail, in other cases, the vortex at the top of the main wing undergoes periodic shedding, which causes large fluctuations in the flow field and affects the generation and disappearance of the vortex at the top of the tail, which in turn leads to the change of the pressure distribution on the surface of the tail and the lift force applied to the tail. In this paper, it is found that if the tail is 1.5m away from the main wing, and the aircraft often does 15° elevation angle manoeuvre during take-off, the tail height design of 0.8m can minimize the tremor on the tail and improve the lift provided by the tail. A tail height of 0.0m-0.2m can also provide better lift and more stable manoeuvring performance.

4 Conclusion

In this paper, based on the Spalart-Allmaras model, Ansys Fluent was used to simulate the effects of different tail heights on the distribution of the mean value of pressure on the tail surface, the distribution of the intensity of pressure fluctuations, and the effect of the tail height on the lift of a small aircraft during manoeuvres at 15° elevation angle. The following conclusions are obtained from the study:

(1) The tail fin in the main wing wake is mainly affected by the airflow disturbance caused by the vortex shedding of the main wing.

(2) The tail surface pressure fluctuation is minimum when the tail is outside the lower boundary of the main wing trailing edge and at the top of the main wing trailing edge.

(3) The lift on the tail is maximum when the tail is at the lower boundary of the main wing trailing edge and at the top of the main wing trailing edge.

This study fills the research gap in this field on the influence of the main wing on the differential pressure force of the tail, and provides help for the design of some low-speed vehicles.

This paper did not discuss the case of different elevation angles and did not model the airframe in three dimensions, ignoring the effect of the airflow disturbance at the wingtip on the tailplane. In the future, it is hoped that a 3D model will be built to discuss in detail the minimum tremor tail position at different elevation angles and the tail position with the best lift to provide more diverse and accurate information for the design of small aircraft.

References

1. Pan D., Cheng J. C.: Unstructured Euler flutter analysis of two-dimensional wing-tail configuration. Journal of aircraft, **32**(5), 1152-1155 (1995)
2. Laschka B., Sensburg O.: Flutter induced by aerodynamic interference between wing and tail. Journal of Aircraft **7**(4), 319-324 (1970)
3. Tuncer I., Platzer M.: Analysis of unsteady airfoil interference effects using a zonal navier-stokes solver. 33rd Aerospace Sciences Meeting and Exhibit. p. 307. Monterey, California, US, (1995)
4. Majeed M. H.: Panel Method Caculations of Wing-Tail Interference Effects. Journal of Engineering **15**(03), 4041-4056 (2009)
5. Jones R. T., Fehlner L F. Transient Effects of the Wing Wake on the Horizontal Tail. 1940.
6. Hoang N. T. B., Bui B. V.: Experimental and numerical studies of wingtip and downwash effects on horizontal tail. Journal of Mechanical Science and Technology 33, 649-659 (2019)
7. McKenna C., Bross M., Rockwell D.: Structure of a streamwise-oriented vortex incident upon a wing. Journal of Fluid Mechanics 816, 306-330 (2017)
8. Qiu J., Sun Q.: Research of aerodynamic load of horizontal tail. 2009 4th IEEE Conference on Industrial Electronics and Applications. pp. 1503-1506. IEEE (2009)
9. Zhang J. D., Zuo Q. H., Lin M. D., et al.: Evolution of vortices in the wake of an ARJ21 airplane: Application of the lift-drag model. Theoretical and Applied Mechanics Letters **10**(6), 419-428 (2020)
10. Spalart, P. R., Allmaras, S. R.: A one-equation turbulence model for aerodynamic flows. Recherche Aerospatiale, **1**, 5–21. (1994)